PLOS COMPUTATIONAL BIOLOGY

RESEARCH ARTICLE

Intraneuronal binding of amyloid beta with reelin—Implications for the onset of Alzheimer's disease

Asgeir Kobro-Flatmoen[1,2]*, **Stig W. Omholt**[3]

1 Kavli Institute for Systems Neuroscience, Norwegian University of Science and Technology (NTNU), Trondheim, Norway, **2** K. G. Jebsen Centre for Alzheimer's Disease, Norwegian University of Science and Technology (NTNU), Trondheim, Norway, **3** Department of Circulation and Medical Imaging, Norwegian University of Science and Technology (NTNU), Trondheim, Norway

* asgeir.kobro-flatmoen@ntnu.no

Citation: Kobro-Flatmoen A, Omholt SW (2025) Intraneuronal binding of amyloid beta with reelin—Implications for the onset of Alzheimer's disease. PLoS Comput Biol 21(1): e1012709. https://doi.org/10.1371/journal.pcbi.1012709

Editor: Fabian Spill, University of Birmingham, UNITED KINGDOM OF GREAT BRITAIN AND NORTHERN IRELAND

Received: June 18, 2024

Accepted: December 9, 2024

Published: January 7, 2025

Peer Review History: PLOS recognizes the benefits of transparency in the peer review process; therefore, we enable the publication of all of the content of peer review and author responses alongside final, published articles. The editorial history of this article is available here: https://doi.org/10.1371/journal.pcbi.1012709

Data Availability Statement: All data are in the manuscript. Instead of depositing the original Python code, we have deposited a CellML version

Abstract

Numerous studies of the human brain supported by experimental results from rodent and cell models point to a central role for intracellular amyloid beta (Aβ) in the onset of Alzheimer's disease (AD). In a rat model used to study AD, it was recently shown that in layer II neurons of the anteriolateral entorhinal cortex expressing high levels of the glycoprotein reelin (Re^{+}alECLII neurons), reelin and Aβ engage in a direct protein–protein interaction. If reelin functions as a sink for intracellular Aβ and if the binding to reelin makes Aβ physiologically inert, it implies that reelin can prevent the neuron from being exposed to the harmful effects typically associated with increased levels of oligomeric Aβ. Considering that reelin expression is extraordinarily high in Re^{+}alECLII neurons compared to most other cortical neurons, such a protective role appears to be very difficult to reconcile with the fact that this subset of ECLII neurons is clearly a major cradle for the onset of AD. Here, we show that this conundrum can be resolved if Re^{+}alECLII neurons have a higher maximum production capacity of Aβ than neurons expressing low levels of reelin, and we provide a rationale for why this difference has evolved.

Author summary

Amyloid-β is a small peptide that is widely recognized as one of the main culprits involved in the development of Alzheimer's disease. It was recently shown that in a subset of neurons in layer II of a brain area called the entorhinal cortex that expresses extraordinarily high levels of the protein reelin, amyloid-β and reelin bind to each other. These neurons, which are strongly involved in memory formation, are among the first to die in subjects with Alzheimer's disease. If intracellular amyloid-β becomes physiologically inert when it binds to reelin, it suggests that reelin can protect these neurons from being exposed to the detrimental effects of increased levels of amyloid-β. Such an effect seems very difficult to reconcile with the fact that these neurons constitute the predominant cortical site for the initiation of Alzheimer's disease. Here, we use a mathematical model to show that this

of the model in the Physiome Model Repository available at: https://models.physiomeproject.org/workspace/be4. We chose this option because the purpose of this repository is both to serve as a permanent store and to allow scientists to share models even if they are using different modeling tools. In addition, a CellML model is curated to ensure consistent use of dimensions and that the provided model and associated parameter values do indeed produce the reported results.

Funding: This work was supported by the Center Grant from (1) The Liaison Committee for Education, Research and Innovation in Central Norway (https://www.helse-midt.no/samarbeidsorganet), (2) The K. G. Jebsen Foundation (http://www.kgjf.org/), The (3) The Kavli Foundation (https://www.kavlifoundation.org/), and (4) and Individual grant from Civitan (https://civitan.no/alzheimerfondet/informasjon-om-fondet/) to AKF. The funders had no role in study design, data collection and analysis, decision to publish, or preparation of the manuscript.

Competing interests: The authors have declared that no competing interests exist.

paradox may be resolved if we allow neurons expressing high levels of reelin to have a higher maximum capacity to produce amyloid-β.

Introduction

Alzheimer's disease (AD) is a neurodegenerative brain disease that causes dementia, and the small peptide amyloid-β (Aβ) and hyperphosphorylated versions of the tau protein (p-tau) have been identified as central in the development of the disease. Studies of large human cohorts strongly suggest that the disease begins with an increase in Aβ in the brain, leading to the generation of p-tau and eventually the formation of insoluble p-tau aggregates, called neurofibrillary tangles (NFTs) [1, 2].

The vast majority of AD subjects experience progressive impairment of declarative memory, whose function depends on the medial temporal lobe memory system. A pivotal component of this system is the entorhinal cortex (EC), which constitutes the main gateway for information flow between the neocortex and the hippocampus and plays a crucial role in the formation, consolidation, and retrieval of memories and spatiotemporal representations. Long before clinically recognized symptoms of AD appear, such as substantial or persistent memory loss, EC is already severely degenerated [3, 4], most notably in its anteriolateral portion (alEC) [5, 6]. Discovering the mechanisms responsible for this impairment is arguably of considerable importance if we want to achieve a truly efficient therapy against AD.

The function of the large glycoprotein reelin in adult mammalian brains includes synaptic modulation, induction of enhanced spine density, and promotion of long-term potentiation [7]. Most neurons in layer II of alEC are unique among cortical excitatory neurons by expressing extraordinally high levels of reelin (dubbed Re^{+}alECLII neurons in the following). In terms of existing data and interpretations of AD development, at least three possibly interlinked paradoxes are attached to this observation.

Numerous studies of the human brain using live imaging, immunohistochemistry, and biochemistry, supported by experimental results from rodent and cell models, point to a role for intracellular Aβ in non-fibrillated forms in the onset of Alzheimer's disease [1]. The first paradox arises from the recent observation that in Re^{+}alECLII neurons in wild type rats as well as in McGill-R-Thy1-APP homozygous transgenic rats (a model commonly used to study AD), reelin and intracellular Aβ engage in a direct protein–protein interaction [8]. This is an intriguing discovery, as it suggests that reelin can function as a sink for intracellular Aβ. If we assume that the Aβ-reelin complex is physiologically inert, this would imply that ECLII neurons with a high reelin level would be better protected from the detrimental effects associated with increased intracellular Aβ expression. However, this does not resonate with the observation that these neurons are among the first to die when the AD phenotype unfolds.

The second paradox arises from our current knowledge of reelin signaling and p-tau formation. Reelin is probably important for the formation of declarative memories, and when it binds to its main receptor in the brain, the apolipoprotein E receptor 2 (ApoER2), it triggers a signaling cascade that increases glutamatergic transmission [7]. Additionally, the binding of reelin to ApoER2 activates a signaling cascade that strongly inhibits the activity of glycogen synthase kinase 3β (GSK3β) [9–11]. GSK3β is one of the main kinases that phosphorylates tau, and constitutive tau phosphorylation causes NFT formation. It has been experimentally demonstrated that interaction with Aβ reduces the capacity of reelin to inhibit GSK3β kinase activity [12]. This suggests that a high intracellular reelin level would buffer against NFT formation in a senescent physiology that causes frequent bouts of increased expression of Aβ. However,

this does not appear to agree with the observation that Re^{+}ECLII projection neurons that reside superficially in layer II are typically the first to form NFTs [2, 13, 14].

The third paradox arises from the relationship between the reelin function and the frequently advocated hypothesis that infectious agents contribute to the pathogenesis of AD. That infections can cause AD has been a controversial issue for decades. However, in the last decade, a substantial body of data has accumulated that at least supports the notion that Aβ has antiviral [15, 16] and antimicrobial properties [17, 18]. And the data support that Aβ oligomers are capable of binding to viruses [16, 19] and microbes [20]. Furthermore, the antimicrobial properties of Aβ have been reported to be similar to the canonical human antimicrobial peptide LL-37, showing an antimicrobial activity equivalent to or, in some cases, superior to this cathelicidin [21] against various clinically relevant bacteria [17]. Therefore, several researchers have proposed that Aβ participates in an immune response to acute microbial or viral infection of the brain [22–25]. Assuming that such an immune response would trigger an increase in the expression of Aβ during pathogen infection, it follows that in Re^{+}alECLII neurons Aβ would be prevented from exerting its immunological function by becoming attached to reelin. Although actual transport mechanisms and subsequent spread of viral infections through the central nervous system (CNS) are still poorly understood [26], the available data clearly suggest that ECLII neurons can be exposed to viral infection through their connection to olfactory receptor neurons and serve as a portal for further CNS infection [26–28]. Furthermore, the EC receives vascular input from the posterior and middle cerebral arteries, which forms particularly dense reticulated networks around individual clusters of ECLII neurons. Together with the neuronal clusters themselves, these networks give rise to characteristic bumps on the surface of the EC, known as the entorhinal verrucae. This redundancy in vascular input suggests that EC may also be particularly exposed to bloodborne pathogens [29]. Due to this propensity to become exposed to pathogens and assuming that increased Aβ production is indeed part of an intraneuronal immune response under native physiological conditions, it does not make evolutionary sense that Re^{+}ECLII neurons should be more vulnerable to pathogen infection than other neurons.

Anticipating that resolving the third paradox may provide clues to resolving the other two, we constructed a simple mathematical model that describes the dynamics between intracellular Aβ, reelin and p-tau formation through the GSK3β pathway as a function of short-term pathogen exposure. We found that if the maximum possible production rate of Aβ is markedly higher in Re^{+}alECLII neurons than in other cortical neurons, Re^{+}alECLII neurons are capable of invoking an immune response similar to that of cortical neurons with low constitutive levels of reelin. This implies that in a senescent physiology predisposing to frequent inflammation-driven Aβ production bursts, also Re^{+}alECLII neurons will be exposed to the detrimental effects of high levels of intracellular Aβ and increased p-tau formation, which resolves the other two paradoxes. Furthermore, we validate the model by showing that it is capable of predicting phenotypic effects associated with two genotypes on opposite sides of the AD risk spectrum, and by showing that it can accurately predict recent experimental data obtained by lowering the level of reelin in Re^{+}alECLII neurons in McGill-R-Thy1-APP rats.

Materials and methods

Description of the dynamic model

The model consists of four differential equations that describe the time rate of change of the number of free intracellular Aβ42 molecules ($[A\beta]$) (the most prominent AD-associated type of Aβ), the number of free intracellular reelin molecules ($[Reelin]$), the number of intracellular Aβ molecules bound to reelin ($[A\beta_{reelin}]$), and the number of phosphorylated GSK3β molecules

being inhibited from inducing hyperphosphorylated tau production ($[GSK3\beta_p]$). The model is used to study the dynamics of these state variables in Re^+alECLII neurons and in cortical neurons that express low levels of reelin (referred to as LR neurons below). The four differential equations are the following.

$$\frac{d[A\beta]}{dt} = \alpha(t) - \beta[A\beta] - \gamma[A\beta][Reelin], \tag{1}$$

$$\frac{d[Reelin]}{dt} = \tau - \rho[Reelin] - \gamma[A\beta][Reelin], \tag{2}$$

$$\frac{d[A\beta_{reelin}]}{dt} = \gamma[A\beta][Reelin] - \delta[A\beta_{reelin}], \tag{3}$$

$$\frac{d[GSK3\beta_p]}{dt} = \eta[Reelin]\left(1 - \frac{[GSK3\beta_p]}{[GSK3\beta_{tot}]}\right) - \kappa[GSK3\beta_p]. \tag{4}$$

If we let $\alpha(t)$ be a constant α, the steady state solution of this system can be expressed in closed form as:

$$[A\beta]^\star = \frac{\alpha\gamma - \beta\rho - \gamma\tau + Q}{2\beta\gamma}, \tag{5}$$

$$[Reelin]^\star = \frac{-\alpha\gamma - \beta\rho + \gamma\tau + Q}{2\gamma\rho}, \tag{6}$$

$$[A\beta_{reelin}]^\star = \frac{\alpha\gamma + \beta\rho + \gamma\tau - Q}{2\delta\gamma}, \tag{7}$$

$$[GSK3\beta_p]^\star = \frac{G_{tot}^2\eta\kappa Q - G_{tot}\eta(G_{tot}\alpha\gamma\kappa + G_{tot}\beta\kappa\rho - G_{tot}\gamma\kappa\tau + 2\beta\eta\tau)}{2G_{tot}^2\gamma\kappa^2\rho - 2G_{tot}\alpha\eta\gamma\kappa - 2G_{tot}\beta\eta\kappa\rho + 2G_{tot}\eta\gamma\kappa\tau - 2\beta\eta^2\tau}, \tag{8}$$

where $Q = \sqrt{\alpha^2\gamma^2 + 2\alpha\beta\gamma\rho - 2\alpha\gamma^2\tau + \beta^2\rho^2 + 2\beta\gamma\rho\tau + \gamma^2\tau^2}$ and $G_{tot} = [GSK3\beta_{tot}]$.

To be precise, the system has an additional steady state solution. But with the parameterization given below, this steady state does not need to be considered, as in this case three of the four state variables have negative values.

Explanation of the differential equations

Eq (1) says that the rate of change of free Aβ is a function of the rate of production of Aβ at time t (α(t)), a first-order decay of Aβ (β = constant) and a second-order binding reaction between Aβ and reelin (γ = constant). We assume a 1:1 binding of reelin to Aβ. Here and in Eqs (2) and (3), the decay term denotes the rate at which the molecular species is tagged for removal. We are agnostic about whether this removal is done by means of the ubiquitin proteasome system, the endosome-autophagosome-lysosome system, the endoplasmic reticulum/Golgi-dependent secretory pathway or by some other process.

Eq (2) says that the rate of change in free reelin is a function of the constitutive production rate of reelin, a first-order decay of free reelin (ρ = constant), and a second-order binding reaction between Aβ and reelin (identical to the last term in Eq (1)). Since in this study we compare the dynamics in two categories of neurons, LR neurons and Re^+alECLII neurons, it rests on the assumption that reelin is present in the vast majority of cortical neurons. To confirm that

this is indeed the case, we performed a quantitative analysis of brain image data from 3, 12 and 18-month-old wild type rats. The analysis showed that almost all of the about 172500 neurons analyzed, located in five different cortical regions, possess a reelin signal that is clearly above the background signal (Fig 1). Due to the high intracellular concentration, it is very likely that reelin is produced in Re^{+}alECLII neurons. However, we do not know whether this is the case in neurons with low constitutive levels of reelin. It may be that the reelin in these cells is delivered by interneurons [30]. If so, the parameter τ will have to be viewed as an import term. However, this does not affect the model as long as low-reelin neurons are provided with about the same amount of reelin per time unit.

Eq (3) says that the rate of change of the amount of the $A\beta_{reelin}$ complex is a function of its production rate (identical to the last term in Eq (1)) and first-order decay of the complex (δ = constant). In this paper, we do not account for the possibility that $A\beta_{reelin}$ complexes aggregate into configurations that may make them less exposed to intracellular degradation or export, which warrants a more complex decay term. Since here we are focused on describing a short-term immune response in native physiology, we can arguably assume that $A\beta_{reelin}$ under this condition is physiologically inert and does not have a notable impact on the formation rates of Aβ or p-tau.

Eq (4) says that the rate of change in the number of phosphorylated GSK3β molecules prevented from inducing tau hyperphosphorylation is given by the rate of GSK3β phosphorylation due to reelin signaling minus a first-order rate process by which phosphorylated GSK3β becomes dephosphorylated (κ = constant). The parameter η is constant and $[GSK3\beta_{tot}]$ is the constitutive number of GSK3β molecules that must be phosphorylated to completely inactivate the GSK3β pathway. The term $(1 - [GSK3\beta_p]/[GSK3\beta_{tot}])$ captures that the phosphorylation rate will decrease with a decrease in the amount of unphosphorylated GSK3β. Reelin inactivates GSK3β by binding to ApoER2 as a dimer [31]. Binding induces a receptor cycle process that activates a signaling cascade that eventually causes the phosphorylation of GSK3β [26], inhibiting its kinase activity. Above a certain level of free reelin, the receptor cycling rate is likely to saturate. It is reason to believe that the functional form of this process is more sigmoidal than hyperbolic because reelin binds to ApoER2 as a dimer and because chemical reactions where one of the reactants is bound to a surface cause so-called fractal kinetics where even reactions involving no cooperativity will behave as they did [32–34]. However, due to the resolution level at which we model, we have not incorporated this mechanism since the term $\eta(1 - [GSK3\beta_p]/[GSK3\beta_{tot}])$ is sufficient to achieve the almost switchlike relationship between $[GSK3\beta_p]^{\star}$ and the reelin concentration that we assume to exist. The rationale being that with such a mechanism, GSK3β remains close to fully phosphorylated beyond a modest free reelin concentration, thus preventing the formation of p-tau. Tau is a signaling hub protein that interacts with a wide variety of kinases and phosphatases, including the Src family kinases cSrc, Fgr, Fyn, and Lck [35]. For example, tau phosphorylation increases its affinity for the tyrosine kinase Fyn [36]. Hence, most likely, p-tau has several functions in native physiology whose orchestration needs to be deliberately regulated. And a switchlike mechanism ensures that the GSK3β pathway is inactivated until its induction is needed, signalled by a substantial reduction in the level of free reelin.

Based on the Fig 1 data, we assume that the two types of neurons we study, Re^{+}alECLII neurons and LR neurons, have identical GSK3β regulation such that the functional relationships that determine the propagation of the signal between reelin and GSK3β are the same. That is, both groups of neurons produce (or receive) sufficient amounts of reelin to suppress the activation of p-tau formation through GSK3β under native physiological conditions, and this suppression begins to fail when the intracellular level of free reelin falls below a certain threshold.

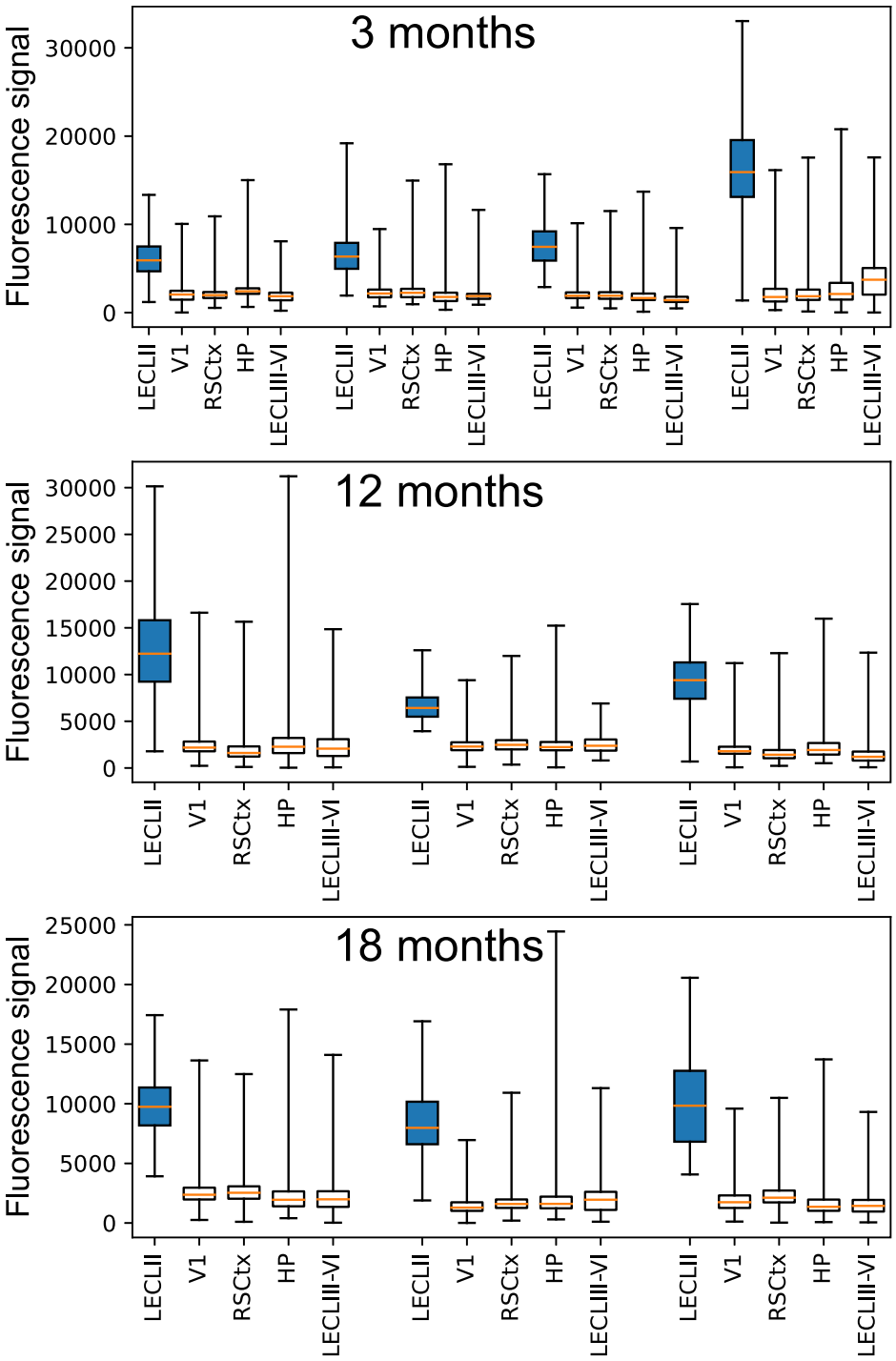

Fig 1. Quantification of reelin levels across cortical regions in wild type rats. Ten animals from three age groups were used in the study (3 months: 4; 12 months: 3; 18 months: 3). Brains were processed as detailed in reference [8]. Briefly, we quantified reelin-levels by way of densitometric measurement of cell profiles (primary antibody = Mouse anti-reelin (G10), Merk, Cat# MAB5364; RRID: AB_2179313; secondary antibody = Alexa 635 Goat anti-mouse (ThermoFisher, Cat# A-31574) in QuPath (Version 0.5.0). For each animal, we randomly selected three sections between Bregma level -5.64 and -6.48 on which the quantifications were done. On these sections, we selected our regions of interest (ROI) to cover the full extent of the cell layers. We adjusted the settings to include the maximum number of detections, such that for each ROI, virtually all available space was separated into unique cell profiles. Then, all cell profiles were assayed. For each section, we measured the signal in the underlying cortical white matter and used this for background subtraction. In rare instances, cell profiles where detected at borders where the tissue was very thin

due to tearing. Occasionally, following background subtraction, these instances gave rise to negative reelin signals (0.02% of the total cell profiles). These cases were deleted from the dataset. In all boxplots, the whiskers cover the whole range of data. LECLII = anteriolateral entorhinal cortex layer II (marked in blue), V1 = primary visual cortex, RSCtx = retrosplenial cortex, HP = hippocampus, LECLIII-VI = anteriolateral entorhinal cortex layers III-VI.

https://doi.org/10.1371/journal.pcbi.1012709.g001

The feedback structure of the model

The Jacobian $\mathbb{J}_{i,j} = \frac{\partial f_i(\mathbf{x})}{\partial x_j}$ of the system is:

$$\mathbb{J}_{i,j} = \begin{bmatrix} -\beta - \gamma x_2 & -\gamma x_1 & 0 & 0 \\ -\gamma x_2 & -\gamma x_1 - \rho & 0 & 0 \\ \gamma x_2 & \gamma x_1 & -\delta & 0 \\ 0 & \eta\left(1 - \frac{x_1}{G_{tot}}\right) & 0 & -\kappa - \frac{\eta x_2}{G_{tot}} \end{bmatrix},$$

where $x_1 = [A\beta]$, $x_2 = [Reelin]$, and $x_4 = [GSK3\beta_p]$.

We see from the Jacobian [37] that the system contains four negative autoregulatory loops (the diagonal elements) and one positive feedback loop between the time rate of change of $[A\beta]$ and the time rate of change of [*Reelin*], i.e. the sign of element (1,2) x element (2,1) is positive. We have found it challenging to further simplify the model without losing essential features.

Linear stability analysis

The Jacobian matrix was also used to study the stability of the baseline steady states of Re^+alECLII neurons and LR neurons given by (Eqs (5)–(8)), using the parameter sets specific to each neuron type (see below). More specifically, we made the above symbolic Jacobian matrix numerical by exchanging the parameter symbols with the numerical parameter values specific for each type of neuron and exchanging the variables x_1, x_2, and x_4 with the baseline steady state values of [Aβ], [Reelin], and [GSK3β_p] specific for each type of neuron (Eqs (5), (6) and (8)). We then calculated the eigenvalues of the two numerical matrices. Since all four eigenvalues in both cases were found to be negative real numbers, the two baseline steady states are locally asymptotically stable. This is also the case for the two steady states obtained when using a high α value to mimic infection, but we do not make use of these steady state values.

Parameterization of the model

Estimation of soma volumes. To keep things simple, we assume the dynamics described by Eqs (1)–(4) is confined to the soma. Given the soma volume, this allows us to translate molecular numbers into molar concentrations. Since different immunohistological methods or subtle differences in the use of the same method can affect the degree of shrinkage of the tissue under investigation, one must be cautious when attempting to compare the size of neuronal somata between different regions of the brain based on published work. With this in mind, we scrutinized the literature to obtain approximate measures of the size of neuronal somata in Re^+alECLII neurons versus LR neurons located in two areas where amyloid plaques tend to appear early in AD, namely the orbitofrontal cortex and the posterior cingulate cortex. In humans, available data [38, 39] suggest that the biggest Re^+alECLII neurons may have somata volumes greater than 12000 μm^3, but often have volumes much lower than this. The largest pyramidal neurons found in the posterior cingulate cortex [40] appear to have somata volumes

greater than 6000 μm^3. For the orbitofrontal cortex, most available data indicate that the volumes of the largest neuronal somata are somewhat lower than this [41, 42], although there are indications that more voluminous somata could be present here [43]. Although alECLII contains neurons with very large somata, they are still not the largest in the cortex, as the somata of pyramidal neurons in layer V can reach volumes many times greater than 12000 μm^3 [44]. We do not know whether the first AD-related changes develop in Re^+alECLII neurons with large or moderate somata volumes. And since the range of soma volume of these neurons overlaps with those of the orbitofrontal cortex and the posterior cingulate cortex, for simplicity, we assumed that the soma volumes of the two neuron groups under study were approximately 4850 μm^3.

Eq (1) parameters. The rate of neuronal secretion of Aβ has been estimated to be in the range of 2-4 $molecules \cdot s^{-1}$ [45], and the ratio of Aβ42 to Aβ40 in the cerebrospinal fluid of young human subjects has been estimated to be approximately 0.15 [46]. Assuming that these figures reflect the baseline levels, we let $\alpha_{baseline} = 1560\ molecules \cdot h^{-1}$ in LR neurons. In healthy Wistar rats, a low level of intracellular Aβ42 is found in neurons throughout the brain at all ages. However, in alECLII neurons, in particular those located in the superficial part of this layer, which is the part that contains the Re^+alECLII neurons, and in hippocampal neurons at the CA1/subiculum border [47], the Aβ42 signal is markedly stronger. We do not have quantitative measurements, but the signal is likely 4-5 times stronger. Due to the phylogenetic conservation of the EC, this pattern is likely to also be present in humans. This notion is supported by available data [47–50]. In accordance with this, we let $\alpha_{baseline} = 7020\ molecules \cdot h^{-1}$ in Re^+alECLII neurons (i.e. 4.5 times that of LR neurons).

We let the half-life of free Aβ in both types of neurons be 6.9 hours, which is 75% of the median half-life of intracellular proteins in mammalian cells [51], giving $\beta = 0.1\ h^{-1}$, and we let the binding rate between reelin and Aβ be $\gamma = 0.005\ molecules^{-1} \cdot h^{-1}$. The results are quite insensitive to the value of γ.

Eq (2) parameters. Since most surface glycoproteins have a half-life of 10-20 hours, and those with protein binding have a median half-life of approximately 19.5 hours [52], we let the free reelin half-life to be 15 hours, giving $\rho = 0.05\ h^{-1}$. Considering the median concentration of signal proteins in the brain is estimated to be 0.087 μM [53], we assumed the free reelin concentration in LR neurons under baseline conditions to be approximately 0.088 μM. With the given values of $\alpha_{baseline}$, β, γ and ρ, it follows from Eqs (5) and (6) that the estimated constitutive production rate (or import rate) of reelin in LR neurons is $\tau = 14500\ molecules \cdot h^{-1}$. Previous experience with immunohistochemical reelin staining [8, 54] indicates that the strong reelin signal obtained from Re^+alECLII neurons reflects a reelin concentration that is at least 5-6 times higher than what is reflected by the signal obtained from LR neurons. We therefore tuned τ so that the steady state reelin concentration in Re^+alECLII neurons was six times higher (528 nM), giving $\tau = 79000\ molecules \cdot h^{-1}$.

Eq (3) parameters. Assuming the intracellular half-life of $A\beta_{reelin}$ to be somewhat longer than that of Aβ and free reelin, we let it be 35 hours, giving $\delta = 0.02\ h^{-1}$.

Eq (4) parameters. Due to the lack of specific data, we assumed that the half-life of the reelin-induced phosphorylated state of GSK3β is approximately one hour, giving $\kappa = 0.65\ h^{-1}$. The estimated K_d value of reelin binding to its receptors is approximately 0.5 nM [9, 55], and to ensure a maximum effect of reelin signaling, the concentration of reelin must be several times higher [56]. Since experiments with embryonic brain cells derived from homozygous *RELN* mice suggest that the addition of 350-700 pM reelin to the medium can induce substantial phosphorylation of GSK3β [57], this indicates that the surface density of ApoER2 in LR neurons is moderate. Due to this, we assumed it to be 36 $molecules \cdot \mu M^{-2}$, which implies G_{tot} ($[GSK3_{tot}]$) = 50000. If Re^+alECLII neurons had the same value G_{tot}, it would mean that the

Table 1. Parameter values used to describe LR and Re$^+$alECLII neurons. Note that the $\alpha_{infection}$ value for Re$^+$alECLII neurons was found by demanding that the maximum $[A\beta]$ level during infection should be about the same as for LR neurons. See main text for further explanation.

	LR neurons	Re$^+$alECLII neurons	Units
$\alpha_{baseline}$	1560	7020	$molecules \cdot h^{-1}$
$\alpha_{infection}$	44000	109000	$molecules \cdot h^{-1}$
β	0.1	0.1	h^{-1}
γ	0.005	0.005	$molecules^{-1} \cdot h^{-1}$
τ	14500	79000	$molecules \cdot h^{-1}$
ρ	0.05	0.05	h^{-1}
δ	0.02	0.02	h^{-1}
η	12	12	h^{-1}
G_{tot}	50000	250000	$molecules$
κ	0.65	0.65	h^{-1}

https://doi.org/10.1371/journal.pcbi.1012709.t001

response time would be considerably higher than that of LR neurons in terms of how fast the cell can ramp up its rate of p-tau production associated with an increase in the rate of Aβ production. Therefore, we would expect that G_{tot} is higher in these neurons. In fact, this seems to be the case [58], and we consequently let $G_{tot} = 250000$, giving an ApoER2 surface density of 180 $molecules \cdot \mu M^{-2}$. This density is still quite moderate compared to the density of several surface receptors [59–61]. We let $\eta = 12\ h^{-1}$ to obtain a baseline proportion of phosphorylated GSK3β of approximately 99% in both groups of neurons.

For convenience, all the parameter values above are compiled in Table 1.

Software used

The model was coded in Python in a Jupyter lab environment. The SymPy Python library [62] was used to calculate closed-form expressions for the steady states of the four state variables under the baseline condition with a low and constant α value. The SciPy Python library [63] was used to study the time evolution of the differential equation system (Eqs (1)–(4)) (scipy.integrate.solve_ivp with the Radau solver).

Results and discussion

Mimicking an immune response in the two groups of neurons

Assuming that Aβ is an important player in an intraneuronal immune response against pathogen infection under native physiological conditions, and based on what we now know about the relationship between reelin and Aβ and the relationship between reelin and p-tau formation, we believe that the following scenario is likely to apply in most cortical neurons:

The production of Aβ is very low as long as the cell does not detect any infection and there will be a marginal accumulation of $A\beta_{reelin}$ complexes. An infection will induce an abrupt increase in the production of Aβ. This will lead to increased accumulation of $A\beta_{reelin}$, depletion of the free reelin level, increase of the free Aβ level, and marked formation of p-tau. After eliminating the pathogen, the cell reduces Aβ levels back to baseline, allowing for a restoration of the original levels of free reelin and $A\beta_{reelin}$ and prevention of further p-tau formation through the reelin-GSK3β pathway.

The *RELN* promoter appears to be under epigenetic control [64], but we assume that this is not relevant in our case. And we assume that reelin production is not under autoregulatory feedback control such that binding to Aβ is not homeostatically compensated for by enhanced

reelin production. The reason being that binding between Aβ and reelin is likely to have a distinct physiological function in native physiology by allowing activation of the GSK3β pathway.

To assess how well the dynamic model was capable of recapitulating the above scenario in cortical neurons with high or low levels of constitutively produced reelin, we initially let a neuron produce Aβ ($\alpha(t)$) at a constant low rate, as described. The initial values of the four state variables at time t_0 were set identical to the steady state values under the given parameter regime (Eqs (5)–(8)). At an arbitrary time t_1 (50 hours), we assumed that the cell detects a pathogen invasion and immediately increases its Aβ production rate to a constant level several times higher. Except for presuming its existence, we were agnostic about the details of the sensing mechanism and how it induces an increase in Aβ production. At time t_2 (170 hours), we assumed that the cell detects that the pathogen has been eliminated and let the production rate of Aβ immediately return to the low basal level. We assumed that the infection lasted five days. However, this figure is not decisive, as a shorter or longer duration will only affect the size of the accumulated $A\beta_{reelin}$ pool and therefore the time it will take before the pool size returns to normal levels after the cessation of infection.

Since our main objective was to identify the prerequisites for achieving a sensible and similar immune response in both types of neurons under the assumption that the basic regulatory architecture is the same, this very simple way of describing a hypothetical immune response is arguably fit for purpose.

Predicted immune response in LR neurons. To mimic the onset of the immune response in LR neurons after 50 hours, we increased the baseline Aβ production rate to $\alpha_{infection} = 44000\ molecules \cdot h^{-1}$ to obtain an assumed Aβ steady state concentration of 100 nM. By this procedure, the model produced an immune response pattern (Fig 2) fully in line with the scenario described above. It should be emphasized that this pattern is obtained even when we let $\alpha_{infection} = 15000\ molecules \cdot h^{-1}$, giving a Aβ steady state concentration of 1.8 nM. However, the Aβ concentration level during infection is likely to be much higher than this [65]. In any case, this shows that the immune response pattern shown in Fig 2 can be achieved by a wide range of $\alpha_{infection}$ values, implying that the current lack of experimental measurements of this parameter is not critical.

Predicted immune response in Re^+alECLII neurons. In Re^+alECLII neurons, we had to increase the Aβ production rate to $\alpha_{infection} = 109000\ molecules \cdot h^{-1}$ to obtain a Aβ steady state concentration of 100 nM (Fig 3). Comparing Figs 2 and 3, we see that the main difference is that the predicted level of $A\beta_{reelin}$ is more than five times higher in Re^+alECLII neurons than in LR neurons. If cortical neurons possess an intraneuronal immune response against pathogens, the model suggests that a prerequisite for Re^+alECLII neurons to produce an immune response on par with cells that have much lower constitutive levels of reelin is that they have a production rate of Aβ that is approximately 2.5 times higher during infection. For both groups of neurons, the model predicts that during infection there will be a conspicuous drop in the amount of free reelin and a pronounced increase in the amounts of Aβ and $A\beta_{reelin}$ (Figs 2 and 3).

Validation of the model

We believe that all predictions provided by Figs 2 and 3 can be conclusively tested by infecting wild type rodents with, for example, herpes simplex virus 1 (HSV1) [26] and measuring the levels of free reelin, free Aβ and $A\beta_{reelin}$ before, during and after infection by existing immunohistochemical protocols [8]. Unfortunately, to the best of our knowledge, such data are not yet available. In the following, we provide a preliminary validation by two different approaches. The first shows that the model is capable of recapitulating observations associated with two contrasting genetic backgrounds, one preventing and one promoting AD development. The

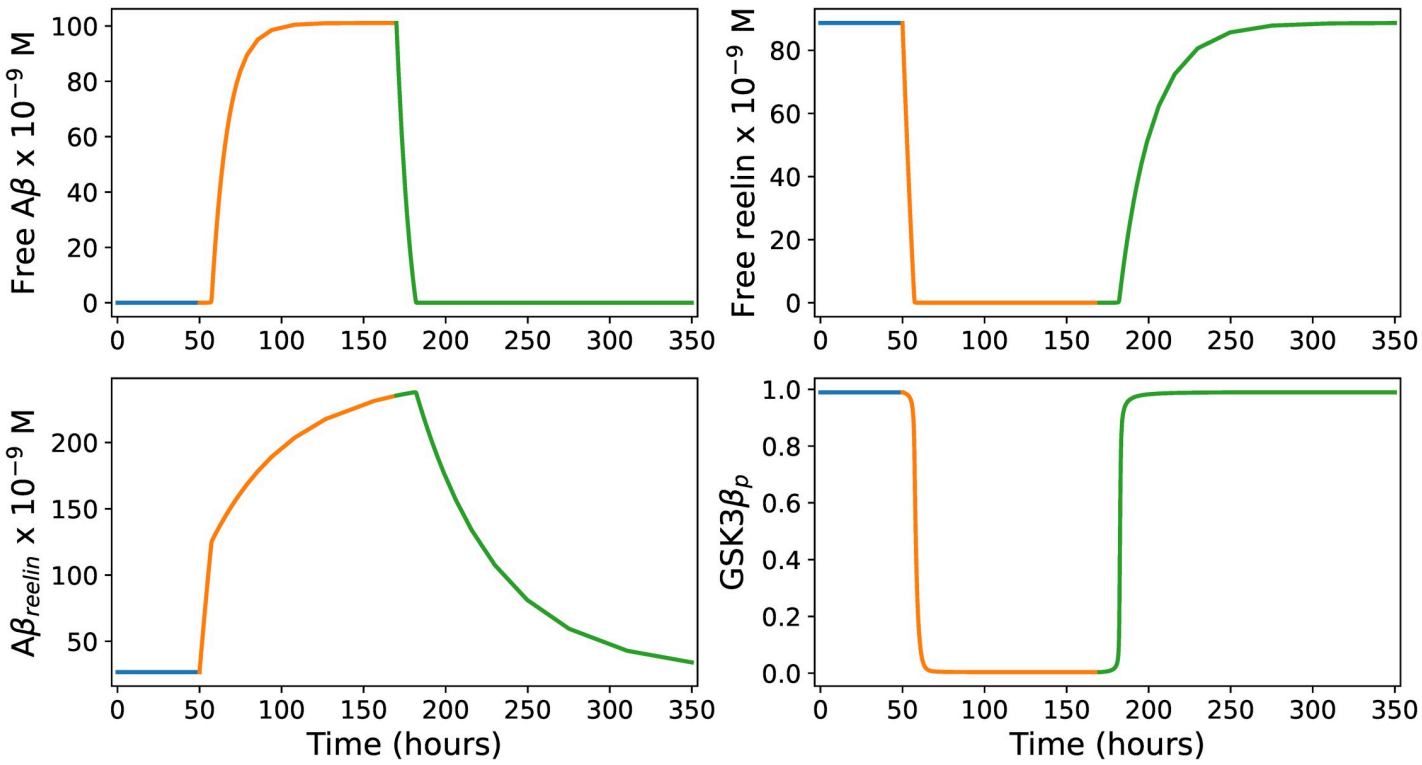

Fig 2. Immune response in LR neurons. The four panels show how the levels of free Aβ, free reelin, $A\beta_{reelin}$ and the proportion of phosphorylated GSK3β relative to the total amount of GSK3β (G_{tot}) develop during an infection event lasting 120 hours (from t = 50 to t = 170). The blue, orange, and green colors describe the pre-infection, infection, and post-infection phases, respectively. See the main text for further explanation.

https://doi.org/10.1371/journal.pcbi.1012709.g002

second shows that the model can predict recent experimental data obtained by lowering the level of reelin in Re^+alECLII neurons in McGill-R-Thy1-APP rats.

The effect of genotype on the immune response in Re^+alECLII neurons. The recently discovered 'COLBOS' genotype, which refers to a rare mutation in the *RELN* gene that encodes reelin, has been shown to cause extreme resilience to AD even when the carrier also possesses the autosomal dominant familial AD (FAD) PSEN1-E280A mutation [66]. The *RELN* mutation clearly helps EC neurons maintain a level of functional reelin that is sufficient to prevent the formation of p-tau, despite being exposed to a high Aβ load [66]. One possible explanation is that the mutation causes a dramatic reduction in the affinity between Aβ and reelin. Thus, letting the value of the parameter γ (Eqs (1), (2) and (3)) become much less than that used to produce Figs 2 and 3, while keeping all other parameters fixed and not including the effect of the PSEN1-E280A mutation, the model can be used to predict the effect of this mutation.

As above, we allowed Re^+alECLII neurons to remain at baseline steady state levels for 50 hours before changing the Aβ production rate from its base level to its maximum level for 120 hours. The model predicts that the level of free Aβ will increase approximately twofold compared to ApoEϵ3/ϵ3 Re^+alECLII neurons, and that the $A\beta_{reelin}$ level will be approximately halved (Fig 4). However, the most notable prediction is that GSK3β will practically remain inhibited during infection, preventing p-tau formation. This is in complete agreement with the notion that the *RELN* mutation prevents p-tau formation by reducing the affinity between reelin and Aβ, causing the level of free reelin to stay above the threshold necessary to inhibit the activity of GSK3β kinase even when the neuron is exposed to a severe free Aβ burden [66].

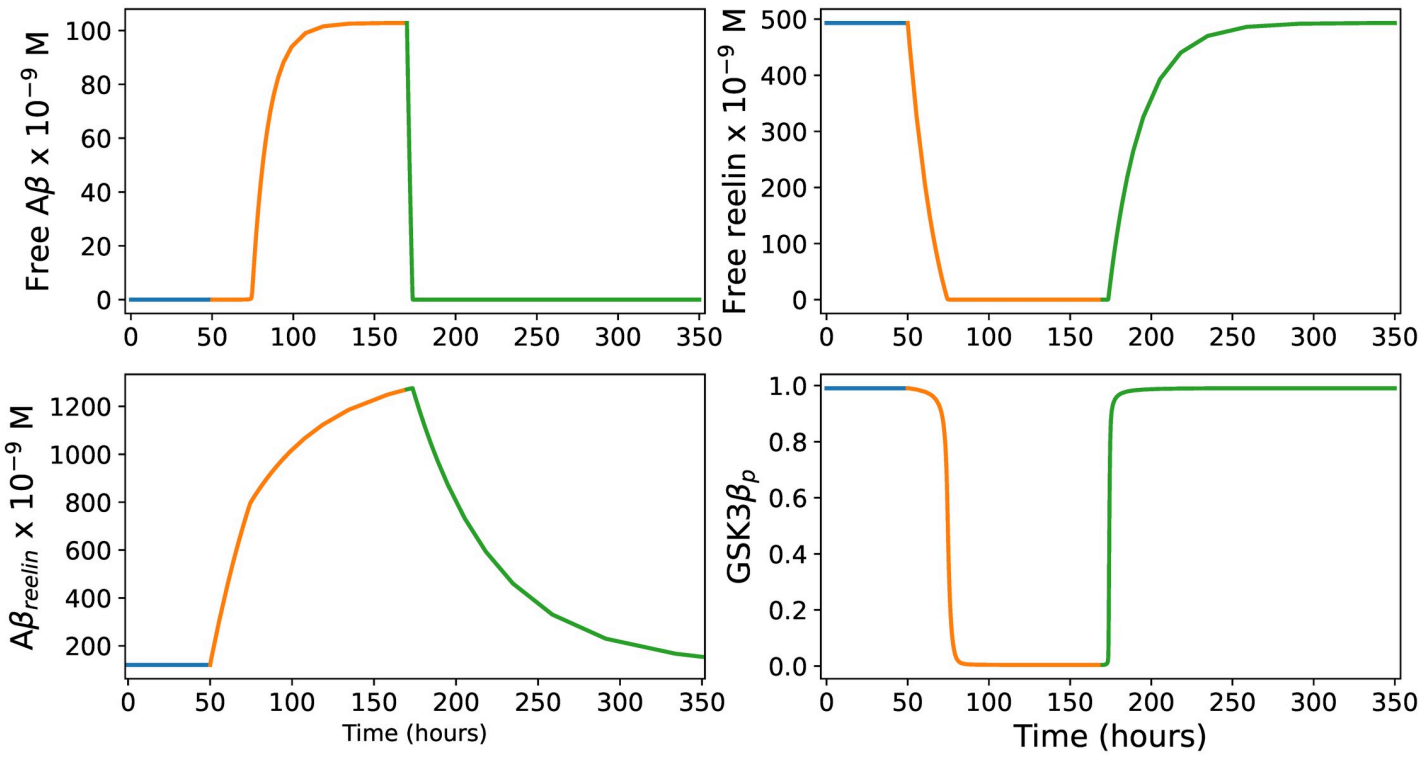

Fig 3. Immune response in Re$^+$alECLII neurons. The four panels show how the levels of free Aβ, free reelin, $A\beta_{reelin}$ and the proportion of phosphorylated GSK3β relative to the total amount of GSK3β (G_{tot}) develop during an infection event lasting 120 hours (from t = 50 to t = 170). See the main text for further explanation.

https://doi.org/10.1371/journal.pcbi.1012709.g003

On the opposite side of the COLBOS genotype in the AD risk spectrum, we have the ApoEϵ4/ϵ4 genotype. The propensity to develop sporadic AD is at least eight times higher in this genetic background than in the most common ApoE genotypic background (ApoEϵ3/ϵ3) [67]. This makes the ApoEϵ4/ϵ4 genotype the most pronounced genetic risk factor for the acquisition of sporadic AD. The causal basis for the observed difference between ApoEϵ4/ϵ4 and ApoEϵ3/ϵ3 subjects has become a much debated issue, and there are numerous attempts at explanations in the literature [68]. Reelin signaling involves endocytosis of ApoER2 receptors. ApoE isoforms differentially affect the recycling of these endosomes, where ApoEϵ3-containing endosomes readily recycle back to the surface, while those containing ApoEϵ4 tend to stall in the vesicles [69]. Here, we assume that this vesicle stalling causes some reelin to be removed from the circulation. Due to the lack of data on cycling rates, we simply mimicked this process by increasing the decay constant ρ to 0.2 in Eq (2).

In the ApoEϵ4/ϵ4 background, the model predicts that the baseline steady state level of free reelin in Re$^+$alECLII neurons will be markedly reduced (Fig 5). However, the most conspicuous prediction is that GSK3β phosphorylation will be less effective under baseline conditions. Given that the effect of vesicle stalling is sufficiently large, this implies that subjects carrying this genotype will have a higher constitutive production of p-tau that over years may have a substantial pathophysiological impact. It remains to be determined how important this effect is compared to other functional effects of the ApoEϵ4/ϵ4 genotype. However, it suggests that the vesicle stalling caused by this genotype may be of importance. And, considering that removal of tau reduces the formation of amyloid plaques in mouse models [70], our results are

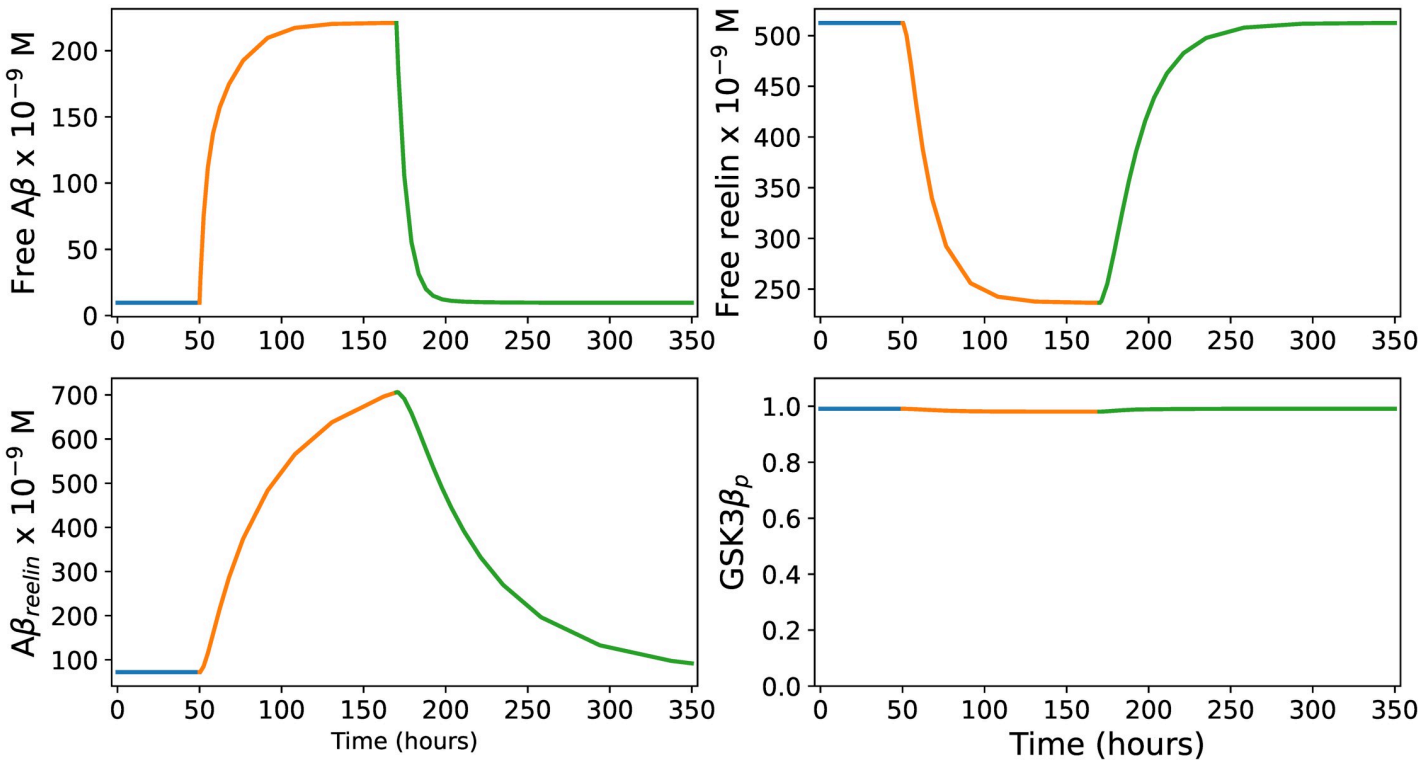

Fig 4. Immune response in Re$^+$alECLII neurons with the COLBOS reelin mutation. The parameter values are identical with those of the ApoEϵ3/ϵ3 genotype, except that γ=0.0000001, i.e., we assume that the reelin mutation is genetically dominant and causes a dramatic reduction in affinity between reelin and Aβ. The four panels show how the levels of free Aβ, free reelin, $A\beta_{reelin}$ and the proportion of phosphorylated GSK3β develop during an infection event lasting 120 hours (from t = 50 to t = 170). See the main text for further explanation.

https://doi.org/10.1371/journal.pcbi.1012709.g004

consistent with the fact that ApoEϵ4/ϵ4 genotypes are characterized by an extremely elevated amyloid plaque burden [71].

Much as the model is capable of recapitulating key features associated with these two genetic backgrounds, which arguably to some degree validates the model as such, much stronger experimental confirmation of the model predictions is of course needed. Conditional on the availability of human neuronal cell cultures in which neurons express a phenotype very similar to Re$^+$alECLII neurons [72], the above predictions can be tested in a setting where cells carrying ApoEϵ4/ϵ4, ApoEϵ3/ϵ3 and COLBOS genotypes are temporarily exposed to a substantially increased intracellular level of Aβ.

Predicting the effect of lowering the level of reelin in Re$^+$alECLII neurons. The test data (Fig 6A and 6B) were taken from a recent experimental study in McGill-R-Thy1-APP homozygous transgenic rats [8]. These rats carry a transgene containing human APP751 with Swedish double mutations and Indiana mutations expressed under the control of the murine Thy1.2 promoter. The transgene causes an increase in the basal production rate of Aβ and an increase in the fraction of Aβ42. Here we just briefly sketch how the test data were generated, since all experimental protocols are given in reference [8].

The reelin level was reduced by injecting Re$^+$alECLII neurons with an adeno-associated viral vector (AAV) expressing miRNA against reelin into the left or right alEC of five one month old McGill-R-Thy1-APP rats. For each injection, the control vector was injected into the contralateral alEC. Reelin levels and Aβ42 levels in experimental neurons (N = 820) and

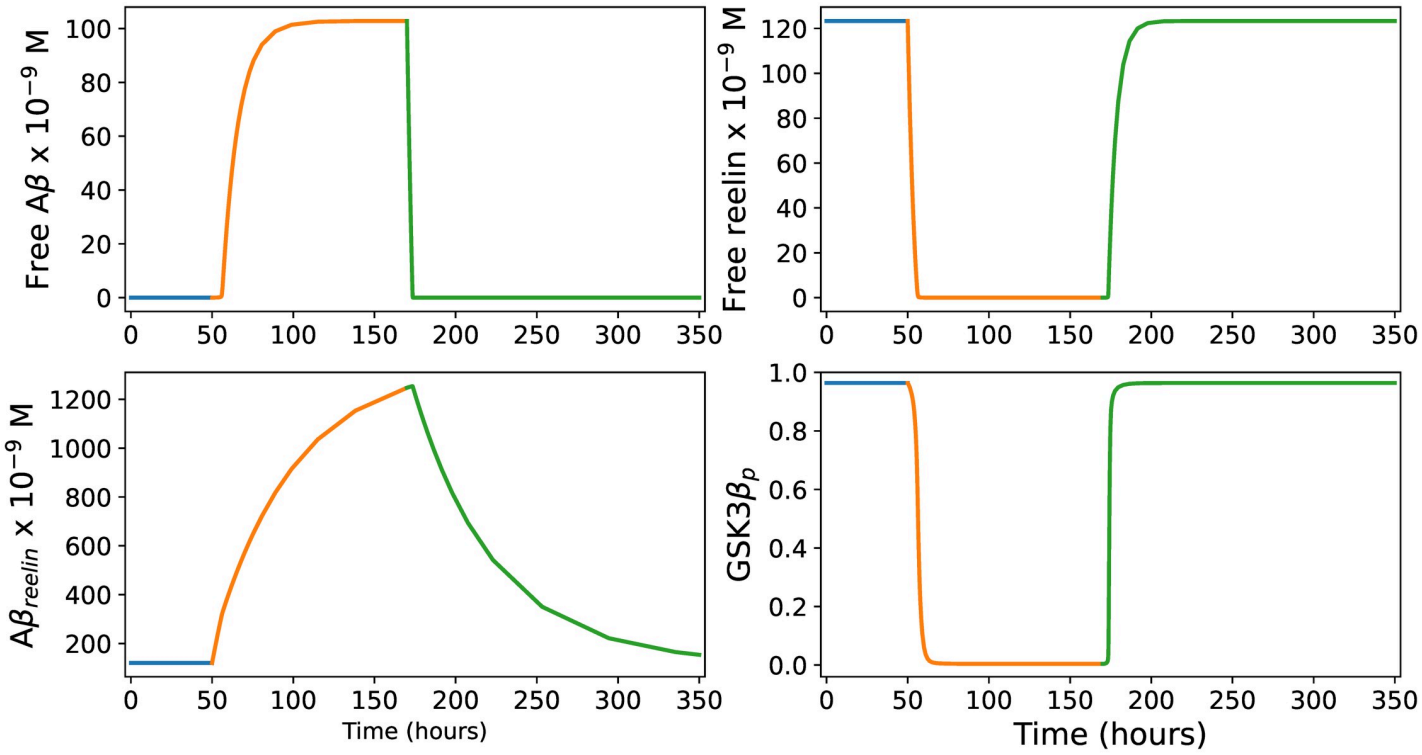

Fig 5. Immune response in ApoEϵ4/ϵ4 Re$^+$alECLII neurons. The parameter values for the ApoEϵ4/ϵ4 genotype are identical with those of the ApoEϵ3/ϵ3 genotype, except that ρ=0.2. The four panels show how the levels of free Aβ, free reelin, $A\beta_{reelin}$ and the proportion of phosphorylated GSK3β develop during an infection event lasting 120 hours (from t = 50 to t = 170). See the main text for further explanation.

https://doi.org/10.1371/journal.pcbi.1012709.g005

control neurons (N = 585) were quantified by fluorescence densitometry when the animals were two months old. The mean levels of reelin and of Aβ42 were in the experimental group of neurons measured as 26% (Fig 6A) and 69% (Fig 6B) of the mean levels in the control group, respectively.

To test whether the model could generate the above two percentage figures, we kept all parameter values used in the wild type Re$^+$alECLII neuron case (Table 1) unchanged except for the baseline production rate of Aβ42 ($\alpha_{baseline}$) and the production rate of reelin (τ). The value of $\alpha_{baseline}$ was changed to account for the effect of the transgene in McGill-R-Thy1-APP rats, and the value of τ was changed to account for the effect of miRNA intervention. It should be noted that the test rests on the assumption that the given parameterization of Eqs 1, 2 and 3 also apply to rats. That is, we assume that the decay rates (β, ρ, δ) and the binding rate between Aβ42 and reelin (γ) are about the same and that the ratio between the baseline production rates of Aβ42 (α) and reelin (τ) is approximately the same in humans and wild type rats.

We do not know exactly how much larger the baseline production rate of Aβ42 is in McGill-R-Thy1-APP Re$^+$alECLII neurons relative to that of wild type. However, based on the expression level of the transgene [73] and existing reports that include measurements of Aβ42 [74, 75], we can confidently assume that it will be in the range of 2-10 times that of wild type alECLII neurons (Table 1). The miRNA-driven reduction of the reelin mRNA pool can be directly translated into a reduced reelin production rate (τ), and we allowed τ to vary in the range 5-100% of the wild type value.

In the control neuron case, we then calculated an array of possible steady states of the total copy number of reelin (using Eq (6) + Eq (7)) and the total copy number of Aβ42 (using Eq (5)

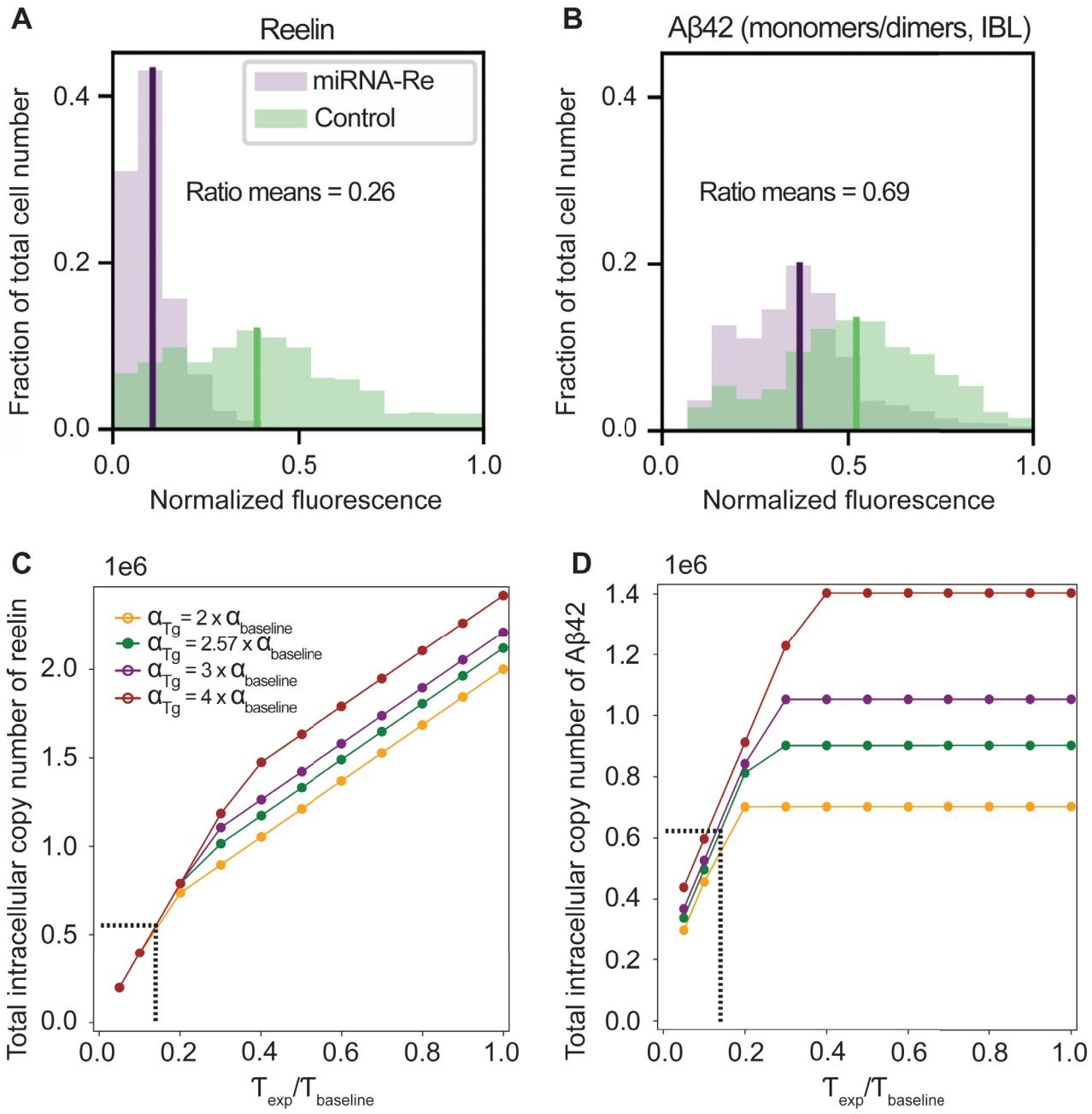

Fig 6. Recapitulating the effects of miRNA intervention in Re$^+$alECLII neurons of McGill-R-Thy1-APP rats. Panels A and B are identical with panels 1 and 4 in Fig 4A in reference [8]. The black vertical lines denote the mean values of the distributions in the experimental group of neurons. The green vertical lines denote the mean values of the distributions in the control group of neurons. The ratios of the mean values of the experimental group to the mean values of the control group are 0.26 and 0.69, respectively. C. Predicted steady state total number of reelin in experimental neurons as a function of the fold change of $\alpha_{baseline}$ in transgenic rats (Tg) compared to wild type and the fractional decrease of τ relative to wild type. Only a small subset of the fold change values and the fractional change values used in the numerical study is shown. The vertical dashed line denotes the predicted fractional reduction in the reelin production rate relative to wild type (0.14) that best fits the data. The horizontal dashed line denotes the total copy number of reelin when the fold change is 2.57. D. Predicted steady state total copy number of Aβ42 in experimental neurons as a function of the fold change of $\alpha_{baseline}$ relative to wild type and the fractional decrease of τ relative to wild type. The horizontal dashed line denotes the total copy number of Aβ42 when the fold change is 2.57.

https://doi.org/10.1371/journal.pcbi.1012709.g006

+ Eq (7)) by letting the fold change of $\alpha_{baseline}$ relative to wild type vary in steps of 0.005 from 2 to 10. In the experimental neuron case, we let $\alpha_{baseline}$ vary in the same way as above. In addition, for each value of $\alpha_{baseline}$, we let the fractional change in τ vary in steps of 0.005 from 0.05 to 1.0. For each step, we calculated the fraction of the total copy number of reelin and Aβ42 in the experimental group relative to the control group. This gave us 304380 records, each containing the fold change in $\alpha_{baseline}$ relative to wild type, the fractional change in τ relative to wild type, and the associated fractions of total reelin and total Aβ42. In this set, we then searched for the record that gave the closest fit to the data.

We found that the model can exactly recapitulate the observed mean fractional decrease in total reelin (0.26) and total Aβ42 (0.69) when the value of τ in the experimental neuron is 14% of the value of the control neuron and $\alpha_{baseline}$ is 2.57 times the value of the wild type (Fig 6C and 6D).

It should be noted that the experimental data only reflect the amount of monomeric and dimeric Aβ42, and we do not know how much was present in the prefibrils or protofibrils. However, we have no apparent reason to believe that the fractions of the three groups differed very much between experimental neurons and control neurons [8] and therefore the reported ratio of monomeric and dimeric Aβ42 (0.69) is likely to be representative of the total amount of Aβ42.

Considering the strong left skewness of the miRNA-Re distribution (Fig 6A) and that its mean value is approximately 12% of the maximal fluorescence level measured, the predicted miRNA-driven reduction in the effective rate of reelin production (14%) appears sensible. To our knowledge, experimental data conclusively supporting or refuting the predicted fold change (2.57) in $\alpha_{baseline}$ are not yet available. However, it is consistent with existing data [73, 74].

The predicted values depend on parameterization. To probe this dependency, we reduced the wild type value of τ in Re^{+}alECLII neurons (Table 1) with 50%. We then repeated the numerical experiment in McGill-R-Thy1-APP rats described above. In this case, the fold change in $\alpha_{baseline}$ must be 1.28 to get the ratio values 0.26 and 0.69. Since this clearly discords with data on the effect of the transgene in McGill-R-Thy1-APP rats [73, 74], it indicates that the value of τ used to produce Fig 2 is not completely off the mark. Due to the current lack of critical experimental data that can be used to further constrain the model parameters, it is nevertheless premature to perform an exhaustive analysis of the relationship between parameter values and the degree to which the model can account for the experimental data in reference [8]. However, the above analysis suggests that this is a worthwhile undertaking to improve the realism of the model as soon as we have better quantitative experimental data, in particular data on the Aβ42 dynamics in Re^{+}alECLII neurons of McGill-R-Thy1-APP and wild type rats.

Taken together, the above results suggest that we are positioned to claim that the model is capable of making predictions that are in clear agreement with the miRNA results on Re^{+}alECLII neurons [8]. This implies that it adequately captures the steady state relationships between Aβ42 and reelin, strongly supporting its main premise, namely that reelin functions as a sink for Aβ42. This, of course, does not serve as a satisfactory validation of the predicted dynamic behavior of the model (Figs 1 and 2). We have alluded to the type of experiments needed to test this behavior. Considering the deliberate simplicity of the model and the uncertainty attached to most of the parameters, it would be surprising if it turned out that new quantitative test data would not require revision of parameter values and adjustments of the model. However, we anticipate that such revisions will not affect our main conclusions.

Concluding remarks

Although it has been established that Aβ has antiviral and antimicrobial properties, it remains to be conclusively shown that Aβ is indeed a major player in a concerted intraneuronal

immune response. But if there is such a response, we claim that Re^{+}alECLII neurons will have to sport a much higher maximum production capacity for Aβ than LR neurons due to their extraordinarily high reelin production. This enhanced production capacity resolves Paradox 3 stated in the Introduction by the fact that it allows Re^{+}alECLII neurons to exert an immune response on the same level as LR neurons. In a senescent physiology predisposing to frequent inflammation-driven Aβ production bursts, the model predicts that Re^{+}alECLII neurons will repeatedly produce enough Aβ to cause the amount of free reelin to drop so much that the formation of p-tau is initiated. Thus, as alluded to, the resolution of Paradox 3 appears to also resolve Paradoxes 1 and 2 stated in the Introduction.

Here, we have deliberately focused on studying the operation of the assumed immune response in native physiology using a very simplistic model. Modeling the effects of a dysfunctional operation of this immune response in a senescent physiology characterized by recurrent inflammation events is a much more challenging undertaking that is beyond the scope of this study. Specifically, this would have to include descriptions of the fate of Aβ, $Aβ_{reelin}$ and p-tau tagged for degradation by the endosome-autophagosome-lysosome system. The disruption of this system consistently appears as an early and progressive characteristic of the pathophysiology of AD [76], leading to the accumulation of degradation-tagged cellular cargo. A solid body of data implicates that the dysfunction of the lysosomal vacuolar (H+)–adenosine triphosphatase (v-ATPase) proton pump is of particular significance and that the amyloid precursor protein (APP) is instrumental in the alkalinization of lysosomes and the subsequent decrease in the lysosomal degradation rate [77–80].

Based on the empirical data available, it is therefore fully conceivable that the degradation of Aβ and $Aβ_{reelin}$ during an inflammation event follows zero-order kinetics instead of first-order kinetics due to the APP-driven reduction of lysosomal degradation capacity. That is, the degradation machinery becomes rapidly saturated, causing a marked increase in the time required to return to baseline levels. This would imply that if the recurrent inflammation events occur frequently and/or last for a prolonged time, the levels of Aβ and $Aβ_{reelin}$ can over years reach pathophysiological levels in terms of soma volume occupancy and subsequent detrimental effects on a variety of cellular processes. This scenario is particularly relevant for the $Aβ_{reelin}$ complex because of the large size of the reelin molecule. This reasoning is supported by experimental data showing that intracellular accumulations of Aβ42 positive material ranged from 20 to 80% of the total cytoplasmic volume in neurons of the entorhinal cortex of patients with sporadic AD [49, 50]. And, as advocated by an increasing number of researchers [48, 49, 81], it points to the possibility that plaque formation can also occur intraneuronally. Thus, given the recurrent dysfunctional activation of the native immune response mechanism studied here, this suggests that the associated long-term effects involve much more than just p-tau seeding. Therefore, we anticipate that if our model is adapted to a senescent physiological context, it may provide crucial information about why ECLII neurons are a cradle for AD.

Acknowledgments

We are very grateful to Sir Peter Hunter and David Nickerson for translating the model into CellML code and making it available on the Physiome Model Repository.

Author Contributions

Conceptualization: Asgeir Kobro-Flatmoen, Stig W. Omholt.

Formal analysis: Asgeir Kobro-Flatmoen, Stig W. Omholt.

Funding acquisition: Asgeir Kobro-Flatmoen.

Methodology: Asgeir Kobro-Flatmoen, Stig W. Omholt.

Project administration: Asgeir Kobro-Flatmoen.

Writing – original draft: Asgeir Kobro-Flatmoen, Stig W. Omholt.

Writing – review & editing: Asgeir Kobro-Flatmoen, Stig W. Omholt.

References

1. Kobro-Flatmoen A, Lagartos-Donate MJ, Aman Y, Edison P, Witter MP, Fang EF. Re-Emphasizing Early Alzheimer's Disease Pathology Starting in Select Entorhinal Neurons, with a Special Focus on Mitophagy. Ageing Res Rev. 2021; 67:101307. https://doi.org/10.1016/j.arr.2021.101307 PMID: 33621703
2. Berron D, Vogel JW, Insel PS, Pereira JB, Xie L, Wisse LEM, et al. Early Stages of Tau Pathology and Its Associations with Functional Connectivity, Atrophy and Memory. Brain. 2021; 144(9):2771–2783. https://doi.org/10.1093/brain/awab114 PMID: 33725124
3. Gómez-Isla T, Price JL, M DW Jr, Morris JC, Growdon JH, Hyman BT. Profound Loss of Layer II Entorhinal Cortex Neurons Occurs in Very Mild Alzheimer's Disease. J Neurosci. 1996; 16(14):4491–4500. https://doi.org/10.1523/JNEUROSCI.16-14-04491.1996 PMID: 8699259
4. Kordower JH, Chu Y, Stebbins GT, DeKosky ST, Cochran EJ, Bennett D, et al. Loss and Atrophy of Layer II Entorhinal Cortex Neurons in Elderly People with Mild Cognitive Impairment. Ann Neurol. 2001; 49(2):202–213. https://doi.org/10.1002/1531-8249(20010201)49:2%3C202::AID-ANA40%3E3.0.CO;2-3 PMID: 11220740
5. Kulason S, Tward DJ, Brown T, Sicat CS, Liu CF, Ratnanather JT, et al. Cortical Thickness Atrophy in the Transentorhinal Cortex in Mild Cognitive Impairment. NeuroImage Clin. 2019; 21:101617. https://doi.org/10.1016/j.nicl.2018.101617 PMID: 30552075
6. Holbrook AJ, Tustison NJ, Marquez F, Roberts J, Yassa MA, Gillen DL, et al. Anterolateral Entorhinal Cortex Thickness as a New Biomarker for Early Detection of Alzheimer's Disease. Alzheimer's & Dementia: Diagnosis, Assessment & Disease Monitoring. 2020; 12(1):e12068. https://doi.org/10.1002/dad2.12068 PMID: 32875052
7. Qiu S, Zhao LF, Korwek KM, Weeber EJ. Differential Reelin-Induced Enhancement of NMDA and AMPA Receptor Activity in the Adult Hippocampus. J Neurosci. 2006; 26(50):12943–12955. https://doi.org/10.1523/JNEUROSCI.2561-06.2006 PMID: 17167084
8. Kobro-Flatmoen A, Battistin C, Nair RR, Bjorkli C, Skender B, Kentros C, et al. Lowering Levels of Reelin in Entorhinal Cortex Layer II-neurons Results in Lowered Levels of Intracellular Amyloid-β. Brain Commun. 2023; 5(2):fcad115. https://doi.org/10.1093/braincomms/fcad115 PMID: 37091586
9. Hiesberger T, Trommsdorff M, Howell BW, Goffinet A, Mumby MC, Cooper JA, et al. Direct Binding of Reelin to VLDL Receptor and ApoE Receptor 2 Induces Tyrosine Phosphorylation of Disabled-1 and Modulates Tau Phosphorylation. Neuron. 1999; 24(2):481–489. https://doi.org/10.1016/S0896-6273(00)80861-2 PMID: 10571241
10. Beffert U, Morfini G, Bock HH, Reyna H, Brady ST, Herz J. Reelin-Mediated Signaling Locally Regulates Protein Kinase B/Akt and Glycogen Synthase Kinase 3β *. J Biol Chem. 2002; 277(51):49958–49964. https://doi.org/10.1074/jbc.M209205200 PMID: 12376533
11. Ohkubo N, Lee YD, Morishima A, Terashima T, Kikkawa S, Tohyama M, et al. Apolipoprotein E and Reelin Ligands Modulate Tau Phosphorylation through an Apolipoprotein E Receptor/Disabled-1/Glycogen Synthase Kinase-3β Cascade. FASEB J. 2003; 17(2):295–297. https://doi.org/10.1096/fj.02-0434fje PMID: 12490540
12. Cuchillo-Ibáñez I, Balmaceda V, Botella-López A, Rabano A, Avila J, Sáez-Valero J. Beta-Amyloid Impairs Reelin Signaling. PLoS One. 2013; 8(8):e72297. https://doi.org/10.1371/journal.pone.0072297 PMID: 23951306
13. Braak H, Braak E. Neuropathological Stageing of Alzheimer-related Changes. Acta Neuropathol. 1991; 82(4):239–259. https://doi.org/10.1007/BF00308809 PMID: 1759558
14. Sanchez JS, Becker JA, Jacobs HIL, Hanseeuw BJ, Jiang S, Schultz AP, et al. The Cortical Origin and Initial Spread of Medial Temporal Tauopathy in Alzheimer's Disease Assessed with Positron Emission Tomography. Sci Transl Med. 2021; 13(577):eabc0655. https://doi.org/10.1126/scitranslmed.abc0655 PMID: 33472953
15. White MR, Kandel R, Tripathi S, Condon D, Qi L, Taubenberger J, et al. Alzheimer's Associated β-Amyloid Protein Inhibits Influenza A Virus and Modulates Viral Interactions with Phagocytes. PLoS One. 2014; 9(e101364):e101364. https://doi.org/10.1371/journal.pone.0101364 PMID: 24988208

16. Bourgade K, Garneau H, Giroux G, Le Page AY, Bocti C, Dupuis G, et al. β-Amyloid Peptides Display Protective Activity against the Human Alzheimer's Disease-Associated Herpes Simplex Virus-1. Biogerontology. 2015; 16:85–98. https://doi.org/10.1007/s10522-014-9538-8 PMID: 25376108
17. Soscia SJ, Kirby JE, Washicosky KJ, Tucker SM, Ingelsson M, Hyman B, et al. The Alzheimer's Disease-Associated Amyloid β-Protein Is an Antimicrobial Peptide. PLoS One. 2010; 5:e9505. https://doi.org/10.1371/journal.pone.0009505 PMID: 20209079
18. Kumar DKV, Choi SH, Washicosky KJ, Eimer WA, Tucker S, Ghofrani J, et al. Amyloid-b Peptide Protects against Microbial Infection in Mouse and Worm Models of Alzheimer's Disease. Sci Transl Med. 2016; 8(340ra72):340ra72. https://doi.org/10.1126/scitranslmed.aaf1059 PMID: 27225182
19. Wozniak MA, Mee AP, Itzhaki RF. Herpes Simplex Virus Type 1 DNA Is Located within Alzheimer's Disease Amyloid Plaques. J Pathol. 2009; 217:131–138. https://doi.org/10.1002/path.2449 PMID: 18973185
20. Spitzer P, Condic M, Herrmann M, Oberstein TJ, Scharin-Mehlmann M, Gilbert DF, et al. Amyloidogenic Amyloid-β-Peptide Variants Induce Microbial Agglutination and Exert Antimicrobial Activity. Sci Rep. 2016; 6:32228. https://doi.org/10.1038/srep32228 PMID: 27624303
21. Vandamme D, Landuyt B, Luyten W, Schoofs L. A Comprehensive Summary of LL-37, the Factotum Human Cathelicidin Peptide. Cell Immunol. 2012; 280(1):22–35. https://doi.org/10.1016/j.cellimm.2012.11.009 PMID: 23246832
22. Fulop T, Witkowski JM, Bourgade K, Khalil A, Zerif E, Larbi A, et al. Can an Infection Hypothesis Explain the Beta Amyloid Hypothesis of Alzheimer's Disease? Front Aging Neurosci. 2018; 10:224. https://doi.org/10.3389/fnagi.2018.00224 PMID: 30087609
23. Butler L, Walker KA. The Role of Chronic Infection in Alzheimer's Disease: Instigators, Co-Conspirators, or Bystanders? Curr Clin Micro Rpt. 2021; 8:199–212. https://doi.org/10.1007/s40588-021-00168-6 PMID: 35186664
24. Wainberg M, Luquez T, Koelle DM, Readhead B, Johnston C, Darvas M, et al. The Viral Hypothesis: How Herpesviruses May Contribute to Alzheimer's Disease. Mol Psychiatry. 2021; 26:5476–5480. https://doi.org/10.1038/s41380-021-01138-6 PMID: 33972690
25. Li F, Hearn M, Bennett LE. The Role of Microbial Infection in the Pathogenesis of Alzheimer's Disease and the Opportunity for Protection by Anti-Microbial Peptides. Crit Rev Microbiol. 2021; 47:240–253. https://doi.org/10.1080/1040841X.2021.1876630 PMID: 33555958
26. van Riel D, Verdijk R, Kuiken T. The Olfactory Nerve: A Shortcut for Influenza and Other Viral Diseases into the Central Nervous System. J Pathol. 2015; 235(2):277–287. https://doi.org/10.1002/path.4461 PMID: 25294743
27. Wouterlood FG, Nederlof J. Terminations of Olfactory Afferents on Layer II and III Neurons in the Entorhinal Area: Degeneration-golgi-electron Microscopic Study in the Rat. Neurosci Lett. 1983; 36(2):105–110. https://doi.org/10.1016/0304-3940(83)90250-1 PMID: 6866324
28. Stroop WG, McKendall RR, Battles EJMM, Schaefer DC, Jones B. Spread of Herpes Simplex Virus Type 1 in the Central Nervous System during Experimentally Reactivated Encephalitis. Microb Pathog. 1990; 8(2):119–134. https://doi.org/10.1016/0882-4010(90)90076-3 PMID: 2161485
29. Stranahan AM, Mattson MP. Selective Vulnerability of Neurons in Layer II of the Entorhinal Cortex during Aging and Alzheimer's Disease. Neural Plast. 2010; 2010:e108190. https://doi.org/10.1155/2010/108190 PMID: 21331296
30. Pesold C, Impagnatiello F, Pisu MG, Uzunov DP, Costa E, Guidotti A, et al. Reelin Is Preferentially Expressed in Neurons Synthesizing γ-Aminobutyric Acid in Cortex and Hippocampus of Adult Rats. Proc Natl Acad Sci USA. 1998; 95(6):3221–3226. https://doi.org/10.1073/pnas.95.6.3221 PMID: 9501244
31. Kubo Ki, Mikoshiba K, Nakajima K. Secreted Reelin Molecules Form Homodimers. Neurosci Res. 2002; 43(4):381–388. https://doi.org/10.1016/S0168-0102(02)00068-8 PMID: 12135781
32. Kopelman R. Fractal Reaction Kinetics. Science. 1988; 241(4873):1620. https://doi.org/10.1126/science.241.4873.1620 PMID: 17820893
33. Savageau MA. Michaelis-Menten Mechanism Reconsidered: Implications of Fractal Kinetics. J Theor Biol. 1995; 176(1):115–124. https://doi.org/10.1006/jtbi.1995.0181 PMID: 7475096
34. Schnell S, Turner TE. Reaction Kinetics in Intracellular Environments with Macromolecular Crowding: Simulations and Rate Laws. Prog Biophys Mol. 2004; 85(2):235–260. https://doi.org/10.1016/j.pbiomolbio.2004.01.012 PMID: 15142746
35. Mueller RL, Combs B, Alhadidy MM, Brady ST, Morfini GA, Kanaan NM. Tau: A Signaling Hub Protein. Front Mol Neurosci. 2021; 14:647054. https://doi.org/10.3389/fnmol.2021.647054 PMID: 33815057
36. Briner A, Götz J, Polanco JC. Fyn Kinase Controls Tau Aggregation In Vivo. Cell Rep. 2020; 32(7):108045. https://doi.org/10.1016/j.celrep.2020.108045 PMID: 32814048

37. Omholt SW, Plahte E. Feedback Confusions. J Theor Biol. 1994; 168(2):231. https://doi.org/10.1006/jtbi.1994.1103

38. Pérez-García CG, González-Delgado FJ, Suárez-Solá ML, Castro-Fuentes R, Martín-Trujillo JM, Ferres-Torres R, et al. Reelin-Immunoreactive Neurons in the Adult Vertebrate Pallium. Journal of Chemical Neuroanatomy. 2001; 21(1):41–51. https://doi.org/10.1016/S0891-0618(00)00104-6 PMID: 11173219

39. Beall MJ, Lewis DA. Heterogeneity of layer II neurons in human entorhinal cortex. Journal of Comparative Neurology. 1992; 321(2):241–266. https://doi.org/10.1002/cne.903210206 PMID: 1500542

40. Vogt BA, Vogt L, Laureys S. Cytology and Functionally Correlated Circuits of Human Posterior Cingulate Areas. NeuroImage. 2006; 29(2):452–466. https://doi.org/10.1016/j.neuroimage.2005.07.048 PMID: 16140550

41. Cotter D, Hudson L, Landau S. Evidence for Orbitofrontal Pathology in Bipolar Disorder and Major Depression, but Not in Schizophrenia. Bipolar Disorders. 2005; 7(4):358–369. https://doi.org/10.1111/j.1399-5618.2005.00230.x PMID: 16026489

42. Haug H, Eggers R. Morphometry of the Human Cortex Cerebri and Corpus Striatum during Aging. Neurobiology of Aging. 1991; 12(4):336–338. https://doi.org/10.1016/0197-4580(91)90013-A PMID: 1961364

43. Jacobs B, Schall M, Prather M, Kapler E, Driscoll L, Baca S, et al. Regional Dendritic and Spine Variation in Human Cerebral Cortex: A Quantitative Golgi Study. Cerebral Cortex. 2001; 11(6):558–571. https://doi.org/10.1093/cercor/11.6.558 PMID: 11375917

44. Meyer G. Forms and Spatial Arrangement of Neurons in the Primary Motor Cortex of Man. Journal of Comparative Neurology. 1987; 262(3):402–428. https://doi.org/10.1002/cne.902620306 PMID: 3655019

45. Moghekar A, Rao S, Li M, Ruben D, Mammen A, Tang X, et al. Large Quantities of Aβ Peptide Are Constitutively Released during Amyloid Precursor Protein Metabolism in Vivo and in Vitro. J Biol Chem. 2011; 286(18):15989–15997. https://doi.org/10.1074/jbc.M110.191262 PMID: 21454701

46. Kim HJ, Lim TS, Lee SM, Kim TS, Kim Y, An YS, et al. Cerebrospinal Fluid Levels of β-Amyloid 40 and β-Amyloid 42 Are Proportionately Decreased in Amyloid Positron-Emission Tomography Negative Idiopathic Normal-Pressure Hydrocephalus Patients. J Clin Neurol. 2019; 15(3):353–359. https://doi.org/10.3988/jcn.2019.15.3.353 PMID: 31286708

47. Kobro-Flatmoen A, Hormann TM, Gouras G. Intracellular Amyloid-β in the Normal Rat Brain and Human Subjects and Its Relevance for Alzheimer's Disease. Journal of Alzheimer's Disease. 2023; 95(2):719–733. https://doi.org/10.3233/JAD-230349 PMID: 37574734

48. Gouras GK, Tsai J, Naslund J, Vincent B, Edgar M, Checler F, et al. Intraneuronal Aβ42 Accumulation in Human Brain. The American Journal of Pathology. 2000; 156(1):15–20. https://doi.org/10.1016/s0002-9440(10)64700-1 PMID: 10623648

49. D'Andrea MR, Nagele RG, Wang HY, Peterson PA, Lee DHS. Evidence That Neurones Accumulating Amyloid Can Undergo Lysis to Form Amyloid Plaques in Alzheimer's Disease. Histopathology. 2001; 38(2):120–134. https://doi.org/10.1046/j.1365-2559.2001.01082.x PMID: 11207825

50. D'Andrea MR, Nagele RG, Wang HY, Lee DHS. Consistent Immunohistochemical Detection of Intracellular β-Amyloid42 in Pyramidal Neurons of Alzheimer's Disease Entorhinal Cortex. Neuroscience Letters. 2002; 333(3):163–166. https://doi.org/10.1016/S0304-3940(02)00875-3 PMID: 12429373

51. Chen W, Smeekens JM, Wu R. Systematic Study of the Dynamics and Half-Lives of Newly Synthesized Proteins in Human Cells. Chem Sci. 2016; 7(2):1393–1400. https://doi.org/10.1039/c5sc03826j PMID: 29910897

52. Xiao H, Wu R. Quantitative Investigation of Human Cell Surface N-glycoprotein Dynamics. Chem Sci. 2017; 8(1):268–277. https://doi.org/10.1039/c6sc01814a PMID: 28616130

53. Shichkova P, Coggan JS, Markram H, Keller D. A Standardized Brain Molecular Atlas: A Resource for Systems Modeling and Simulation. Frontiers in Molecular Neuroscience. 2021; 14. https://doi.org/10.3389/fnmol.2021.604559 PMID: 34858137

54. Kobro-Flatmoen A, Nagelhus A, Witter MP. Reelin-Immunoreactive Neurons in Entorhinal Cortex Layer II Selectively Express Intracellular Amyloid in Early Alzheimer's Disease. Neurobiol Dis. 2016; 93:172–183. https://doi.org/10.1016/j.nbd.2016.05.012 PMID: 27195475

55. Weeber EJ, Beffert U, Jones C, Christian JM, Förster E, Sweatt JD, et al. Reelin and ApoE Receptors Cooperate to Enhance Hippocampal Synaptic Plasticity and Learning *. Journal of Biological Chemistry. 2002; 277(42):39944–39952. https://doi.org/10.1074/jbc.M205147200 PMID: 12167620

56. Hamad MIK, Petrova P, Daoud S, Rabaya O, Jbara A, Melliti N, et al. Reelin Restricts Dendritic Growth of Interneurons in the Neocortex. Development. 2021; 148(17):dev199718. https://doi.org/10.1242/dev.199718 PMID: 34414407

57. Howell BW, Herrick TM, Cooper JA. Reelin-Induced Tryosine Phosphorylation of Disabled 1 during Neuronal Positioning. Genes Dev. 1999; 13(6):643–648. https://doi.org/10.1101/gad.13.6.643 PMID: 10090720

58. Ramsden CE, Zamora D, Horowitz MS, Jahanipour J, Calzada E, Li X, et al. ApoER2-Dab1 Disruption as the Origin of pTau-associated Neurodegeneration in Sporadic Alzheimer's Disease. Acta Neuropathol Commun. 2023; 11:197. https://doi.org/10.1186/s40478-023-01693-9 PMID: 38093390

59. Chen Y, Munteanu AC, Huang YF, Phillips J, Zhu Z, Mavros M, et al. Mapping Receptor Density on Live Cells by Using Fluorescence Correlation Spectroscopy. Chemistry. 2009; 15(21):5327–5336. https://doi.org/10.1002/chem.200802305 PMID: 19360825

60. Patrizio A, Specht CG. Counting Numbers of Synaptic Proteins: Absolute Quantification and Single Molecule Imaging Techniques. Neurophotonics. 2016; 3(4):041805. https://doi.org/10.1117/1.NPh.3.4.041805 PMID: 27335891

61. Zhang F, Wang S, Yin L, Yang Y, Guan Y, Wang W, et al. Quantification of Epidermal Growth Factor Receptor Expression Level and Binding Kinetics on Cell Surfaces by Surface Plasmon Resonance Imaging. Anal Chem. 2015; 87(19):9960–9965. https://doi.org/10.1021/acs.analchem.5b02572 PMID: 26368334

62. Meurer A, Smith CP, Paprocki M, Čertík O, Kirpichev SB, Rocklin M, et al. SymPy: Symbolic Computing in Python. PeerJ Comput Sci. 2017; 3:e103. https://doi.org/10.7717/peerj-cs.103

63. Virtanen P, Gommers R, Oliphant TE, Haberland M, Reddy T, Cournapeau D, et al. SciPy 1.0: Fundamental Algorithms for Scientific Computing in Python. Nat Methods. 2020; 17(3):261–272. https://doi.org/10.1038/s41592-019-0686-2 PMID: 32015543

64. Chen Y, Sharma RP, Costa RH, Costa E, Grayson DR. On the Epigenetic Regulation of the Human Reelin Promoter. Nucleic Acids Research. 2002; 30(13):2930–2939. https://doi.org/10.1093/nar/gkf401 PMID: 12087179

65. Wozniak MA, Itzhaki RF, Shipley SJ, Dobson CB. Herpes Simplex Virus Infection Causes Cellular β-Amyloid Accumulation and Secretase Upregulation. Neurosci Lett. 2007; 429:95–100. https://doi.org/10.1016/j.neulet.2007.09.077 PMID: 17980964

66. Lopera F, Marino C, Chandrahas AS, O'Hare M, Villalba-Moreno ND, Aguillon D, et al. Resilience to Autosomal Dominant Alzheimer's Disease in a Reelin-COLBOS Heterozygous Man. Nat Med. 2023; 29:1243–1252. https://doi.org/10.1038/s41591-023-02318-3 PMID: 37188781

67. Rasmussen KL, Tybjærg-Hansen A, Nordestgaard BG, Frikke-Schmidt R. Absolute 10-Year Risk of Dementia by Age, Sex and APOE Genotype: A Population-Based Cohort Study. CMAJ. 2018; 190(35):E1033–E1041. https://doi.org/10.1503/cmaj.180066 PMID: 30181149

68. Safieh M, Korczyn AD, Michaelson DM. ApoE4: An Emerging Therapeutic Target for Alzheimer's Disease. BMC Med. 2019; 17(1):64. https://doi.org/10.1186/s12916-019-1299-4 PMID: 30890171

69. Morrow JA, Hatters DM, Lu B, Höchtl P, Oberg KA, Rupp B, et al. Apolipoprotein E4 Forms a Molten Globule: A Potential Basis for Its Association with Disease. J Biol Chem. 2002; 277(52):50380–50385. https://doi.org/10.1074/jbc.M204898200 PMID: 12393895

70. Peters F, Salihoglu H, Pratsch K, Herzog E, Pigoni M, Sgobio C, et al. Tau Deletion Reduces Plaque-associated BACE1 Accumulation and Decelerates Plaque Formation in a Mouse Model of Alzheimer's Disease. The EMBO Journal. 2019; 38(23):e102345. https://doi.org/10.15252/embj.2019102345 PMID: 31701556

71. Drzezga A, Grimmer T, Henriksen G, Mühlau M, Perneczky R, Miederer I, et al. Effect of APOE Genotype on Amyloid Plaque Load and Gray Matter Volume in Alzheimer Disease. Neurology. 2009; 72(17):1487–1494. https://doi.org/10.1212/WNL.0b013e3181a2e8d0 PMID: 19339712

72. Bergmann T, Liu Y, Skov J, Mogus L, Lee J, Pfisterer U, et al. Production of Human Entorhinal Stellate Cell-like Cells by Forward Programming Shows an Important Role of Foxp1 in Reprogramming. Front Cell Dev Biol. 2022; 10. https://doi.org/10.3389/fcell.2022.976549 PMID: 36046338

73. Leon WC, Canneva F, Partridge V, Allard S, Ferretti MT, DeWilde A, et al. A Novel Transgenic Rat Model with a Full Alzheimer's-Like Amyloid Pathology Displays Pre-Plaque Intracellular Amyloid-β-Associated Cognitive Impairment. Journal of Alzheimer's Disease. 2010; 20(1):113–126. https://doi.org/10.3233/JAD-2010-1349 PMID: 20164597

74. Iulita MF, Allard S, Richter L, Munter LM, Ducatenzeiler A, Weise C, et al. Intracellular Aβ Pathology and Early Cognitive Impairments in a Transgenic Rat Overexpressing Human Amyloid Precursor Protein: A Multidimensional Study. acta neuropathol commun. 2014; 2(1):61. https://doi.org/10.1186/2051-5960-2-61 PMID: 24903713

75. Flores-Aguilar L, Hall H, Orciani C, Foret MK, Kovecses O, Ducatenzeiler A, et al. Early Loss of Locus Coeruleus Innervation Promotes Cognitive and Neuropathological Changes before Amyloid Plaque Deposition in a Transgenic Rat Model of Alzheimer's Disease. Neuropathology and Applied Neurobiology. 2022; 48(6):e12835. https://doi.org/10.1111/nan.12835 PMID: 35822518

76. Knopman DS, Amieva H, Petersen RC, Chételat G, Holtzman DM, Hyman BT, et al. Alzheimer Disease. Nat Rev Dis Primers. 2021; 7(1):1–21. https://doi.org/10.1038/s41572-021-00269-y

77. Song Q, Meng B, Xu H, Mao Z. The Emerging Roles of Vacuolar-Type ATPase-dependent Lysosomal Acidification in Neurodegenerative Diseases. Translational Neurodegeneration. 2020; 9(1):17. https://doi.org/10.1186/s40035-020-00196-0 PMID: 32393395

78. Jiang C, Chen JS, Li S, Zhang F, Deng J, Zeng LH, et al. Amyloid Precursor Protein: A Regulatory Hub in Alzheimer's Disease. Aging and disease. 2024; 15:201–225.

79. Im E, Jiang Y, Stavrides PH, Darji S, Erdjument-Bromage H, Neubert TA, et al. Lysosomal Dysfunction in Down Syndrome and Alzheimer Mouse Models Is Caused by V-ATPase Inhibition by Tyr682-phosphorylated APP βCTF. Science Advances. 2023; 9(30):eadg1925. https://doi.org/10.1126/sciadv.adg1925 PMID: 37494443

80. Koh JY, Kim HN, Hwang JJ, Kim YH, Park SE. Lysosomal Dysfunction in Proteinopathic Neurodegenerative Disorders: Possible Therapeutic Roles of cAMP and Zinc. Molecular Brain. 2019; 12(1):18. https://doi.org/10.1186/s13041-019-0439-2 PMID: 30866990

81. Lee JH, Yang DS, Goulbourne CN, Im E, Stavrides P, Pensalfini A, et al. Faulty Autolysosome Acidification in Alzheimer's Disease Mouse Models Induces Autophagic Build-up of Aβ in Neurons, Yielding Senile Plaques. Nat Neurosci. 2022; 25(6):688–701. https://doi.org/10.1038/s41593-022-01084-8 PMID: 35654956